Analytic Study of Sea–Land Breezes

K. Young

Department of Physics, The Chinese University of Hong Kong, Hong Kong, China

Zhang Ming① (张 铭)

LASG, Institute of Atmospheric Physics, Chinese Academy of Sciences, Beijing 100080

(Received February 6, 1998)

ABSTRACT

An analytic study of the structure of sea–land breezes is presented, with special attention paid to the dependence on the model parameters. In this linearized model, the wind speed of the sea–land breezes is directly proportional to the difference of sea and land heating rates. For the same differential heating, the sea–land breeze is more prominent if the stratification is weakly stable, or if the frictional force is small. The horizontal penetration from the coast is also investigated, and found to be asymmetric between the land and the sea. The above results are in agreement with observation.

Key words: Sea–land breeze, Analytic model

1. Introduction

Sea–land breezes are mesoscale, secondary circulations forced by thermal gradients, and typically occur under conditions of weak prevailing background winds. In the daytime, the land, with a smaller heat capacity, heats up more than the sea. As a result, the air above the land surface is hotter, and the pressure lower. Wind then blows from sea to land; this is the sea breeze. At night, the situation is reversed, giving rise to the land breeze. Fig. 1 gives the component of the wind perpendicular to the coast above Santa Monica, California (Flohn, 1969), showing a diurnal variation. The wind direction near the surface changes from NE (land breeze) to SW (sea breeze). The speeds are moderate, about several m s^{-1}, with sea breezes somewhat stronger than land breezes. Whether in the sea breeze phase or the land breeze phase, mass conservation demands that there must be a return flow; indeed, above 1.5 km from the surface, the wind direction is reversed, with a relatively low speed.

The sea–land breeze circulation has attracted attention from early days. Halley (1686) studied this phenomenon in 1686. Many other investigations have since been carried out (Sun et al., 1981; Smith et al., 1982; Rotunno, 1983; Niino, 1987; Yan et al., 1987). Recent attention is also related to the dispersal of airborne pollutants, which is important for coastal industrial areas (Lu et al., 1994).

Studies of the sea–land breeze circulation can be classified into observational studies, theoretical studies and numerical modelling. Despite the necessary simplifications, analytic models are important for the insights they provide. Haurwitz (1947) assumed that the pressure gradient force perpendicular to a straight coastline can be expressed as $-\partial\varphi/\partial x$, and

①Corresponding author: LASG, Institute of Atmospheric Physics, Chinese Academy of Sciences, Beijing, China.

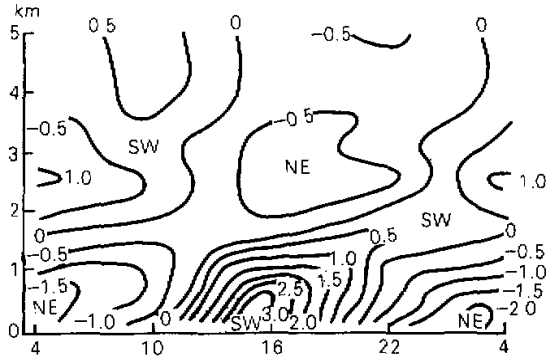

Fig. 1. The component of the wind perpendicular to the coast above Santa Monica, CA, USA, averaged over 29 sea-breeze days. Positive values (m s^{-1}) indicate sea breeze. The horizontal axis is time (expressed in LST) and the vertical axis is height. Taken from Flohn (1969).

varies in time periodically with frequency $\omega = 2\pi / T$, where T is one day. Based on these assumptions, the solution of a linear homogeneous sea-land breeze model was found. Defant (1951) assumed that the perturbation of the surface potential temperature can be written as

$$\theta(x, z = 0, t) = \theta_{\max} e^{i\omega t} \sin lx \ , \tag{1}$$

where x is the coordinate perpendicular to the coast, and z is the vertical height. This parameterization of the x-dependence is somewhat unphysical. Walsh (1974) assumed the perturbation of temperature to be

$$\theta(x, z = 0, t) = \sin\omega t \times \begin{cases} \theta_{\max}, & x > 0 \\ -\theta_{\min}, & x < 0 \end{cases} . \tag{2}$$

The step-function profile in x is more realistic, and solutions were found within a linear homogeneous sea-land breeze model. Both of these models start from the temperature, whereas more realistically one should start with the heating rates as the driving force; the time lag between the heating and the temperature rise should be part of the outcome of the model, and important for understanding the time of onset of sea and land breezes.

Rotunno (1983) reviewed the development of analytic solutions of linear sea-land breeze models. By ignoring the frictional force but incorporating the heating rate in an inhomogeneous sea-land breeze model, an analytic solution was obtained. Dalu and Pielke (1989) analyzed a model with both heating and friction (but with the latter assuming the same value on land and on sea). Up to now, there have been very few models that take the different frictional forces as well as the different heating rates over land and sea into proper account. Some numerical studies considered both effects, as well as non-linear effects (Sun et al., 1981). Many results of observational, analytic and numerical studies were reviewed by Simpson (1994).

The analytic solution of a linear sea-land breeze model is presented in this paper. The model starts with different heating rates over land and sea, and also incorporates different frictional forces on land and sea. The former drives the entire effect, and all measures of the sea-land breeze circulation are proportional to the differential heating; the latter plays some role in controlling the extent of the penetration landwards and seawards. These and other de-

pendences on the model parameters are studied.

The rest of this paper is organized as follows. In Section 2 we develop the mathematical model and solution, expressing all flow fields as a rapidly convergent series. In Section 3 we analyze the structure of the sea–land breeze circulation using a set of "standard" parameters. In Section IV we study how the circulation is affected by changes in these parameters, and the concluding remarks are given in Section 5.

2. Mathematical model and solution

2.1 *Basic equations*

The model domain consists of an infinite horizontal plane with an infinitely long and straight coastline along y axis, separating the land ($x < 0$) from the sea ($x > 0$). The vertical extent is from sea level ($z = 0$) to a maximum height $z = H$, where H will be one of the model parameters. There is no variation along y direction, so the problem reduces to two dimensions in $x - z$ plane. As the sea–land breeze is a mesoscale system, the Coriolis parameter f can be assumed to be constant. The two-dimensional flow is treated in the Boussinesq approximation, and because the wind speeds in sea–land breezes are moderate, the equations are linearized. This results in the following set of governing equations.

$$\frac{\partial u}{\partial t} - fv + \frac{\partial p'}{\partial x} = -ku \ ,$$

$$\frac{\partial v}{\partial t} + fu = -kv \ ,$$

$$\frac{\partial \omega}{\partial t} - \theta + \frac{\partial p'}{\partial z} = -k\omega \ ,$$

$$\frac{\partial \theta}{\partial t} + N^2 w = Q + \xi \frac{\partial^2 \theta}{\partial x^2} \ ,$$

$$\frac{\partial u}{\partial x} + \frac{\partial w}{\partial z} = 0 \ . \tag{3}$$

In the above, u, v are the horizontal components of the wind field, w is the vertical component, $\theta = g(\theta' / \theta_0)$ in which θ' is the potential temperature perturbation, p' is the pressure perturbation, N is the Brunt–Vaisala frequency, k is a Rayleigh frictional parameter, assumed to be constant over each domain, and ξ is the horizontal heat diffusion coefficient, very small in general. For simplicity, we neglect the heat diffusion term in the derivation below. The heating rate Q is determined by the radiation balance, and may be assumed to take the factorized form

$$Q = Q_x(x) Q_z(z) \sum_n q_n e^{in\omega t} \ , \tag{4}$$

where $Q_x(x)$ describes the horizontal distribution perpendicular to the coast and $Q_z(z)$ describes the vertical distribution. The time variation, assumed to be periodic with period $T = 2\pi / \omega = 1$ d, is expanded in harmonics. For simplicity again, only the fundamental ($n = 1$) is kept; moreover, we shall implicitly take the real part, so that $t = 0$ corresponds to

noon. By keeping only the fundamental frequency, the circulation will be exactly reversed in the two halves of a diurnal cycle, so that within this approximation, the land breeze and sea breeze phases will be mirror images, with equal strengths; the limitations of this simplification are discussed in Section 5.

The boundary conditions for Eq.(3) are

$$w|_{z=0} = w|_{z=H} = 0 \ . \tag{5}$$

Clearly all quantities vary at the fundamental frequency ω, so we define amplitudes $\hat{u}$, $\hat{v}$,$\cdots$ by, e.g.,

$$u = \hat{u}e^{i\omega t} \ , \tag{6}$$

where the phases of the amplitudes $\hat{u}$, $\hat{v}$,$\cdots$ represent possible time lags in response. Next we put Eq.(6) into Eq.(3), and introduce the stream function $\hat{\psi}$,

$$\hat{u} = \frac{\partial \hat{\psi}}{\partial z} \ ,$$

$$\hat{w} = -\frac{\partial \hat{\psi}}{\partial x} \ . \tag{7}$$

By eliminating $\hat{p}$, the equations become

$$\begin{aligned}
&(i\omega + k)\hat{v} + f\frac{\partial \hat{\psi}}{\partial z} = 0 \ , \\
&(i\omega + k)\left(\frac{\partial^2 \hat{\psi}}{\partial z^2} + \frac{\partial^2 \hat{\psi}}{\partial z^2}\right) - f\frac{\partial \hat{v}}{\partial z} + \frac{\partial \hat{\theta}}{\partial x} = 0 \ , \\
&i\omega\hat{\theta} - N^2\frac{\partial \hat{\psi}}{\partial x} = q_1 Q_x(x)Q_z(z) \ , \\
&\hat{\psi}|_{z=0} = \hat{\psi}|_{z=H} = 0 \ .
\end{aligned} \tag{8}$$

The heating rate and the frictional force are assumed to be different forms over land and sea; we take

$$q_1 Q_x(x)Q_z(z) = \begin{cases} Q_l e^{-\delta z} \ , & x < 0 \\ Q_s e^{-\delta z} \ , & x > 0 \end{cases} \tag{9}$$

where δ, Q_l and Q_s are constants, with $Q_l > Q_s$. For simplicity, we assume the vertical distribution over land and sea to be characterized by the same scale δ^{-1}. Similarly, the frictional parameter is assumed to be

$$k = \begin{cases} k_l, & x < 0 \\ k_s, & x > 0 \end{cases} \tag{10}$$

which are also constants, with $k_l > k_s$.

The standard set of values we shall use in this paper is given in Table 1.

The strategy is as follows. We first solve the equations in each region ($x < 0$ and $x > 0$); in each case, the solution will consist of a particular solution (respectively proportional to Q_l and Q_s), plus a homogeneous solution, the latter with unknown coefficients. The solutions are then matched across the coastline $x = 0$ to determine the coefficients.

Table 1. The standard values of model parameters

Parameter	Value	Unit	Comments
Q_1	4×10^{-6}	$\mathrm{m\,s^{-3}}$	
Q_2	1×10^{-6}	$\mathrm{m\,s^{-3}}$	
k_1	5	$\mathrm{day^{-1}}$	
k_s	1.25	$\mathrm{day^{-1}}$	$k_s = 0.25k_1$
N^2	1×10^{-4}	$\mathrm{s^{-2}}$	
f	0.54484×10^{-5}	$\mathrm{s^{-1}}$	at latitude 22°N
H	1	km	
δ	2×10^{-3}	$\mathrm{m\,s^{-1}}$	

2.2 *Solution in each region*

The case over land ($x < 0$) and over sea ($x > 0$) will be discussed separately. For $x < 0$, the heating term on the right hand side of Eq.(8) becomes $Q_1 e^{-\delta z}$, and the value of k becomes k_1. The following particular solution

$$\hat{\psi} = 0$$
$$\hat{v} = 0$$
$$\hat{\theta} = -\frac{i}{\omega} Q_1 e^{-\delta z} \tag{11}$$

describes a static flow field with the potential temperature varying at the same frequency as the external heating source, but lagging by 1 / 4 cycle (6 hours).

Next, consider the general homogeneous solution. Since the vertical extent is $0 < z < H$, the z-dependence of the heating terms $e^{-\delta z}$ can be expanded in a Fourier series involving $\sin(m\pi z / H)$, $m = 1,2,\cdots$; see Eq.(18) below①. Thus all the unknown functions can also be expanded in Fourier series in z; moreover, it is easily seen that the x-dependence must be exponential, so②

$$\hat{u} = \sum_{m=1}^{\infty} U_{lm} e^{\beta_{lm} x} \cos(m\pi z / H) ,$$
$$\hat{v} = \sum_{m=1}^{\infty} V_{lm} e^{\beta_{lm} x} \cos(m\pi z / H) ,$$
$$\hat{\psi} = \sum_{m=1}^{\infty} \Psi_{lm} e^{\beta_{lm} x} \sin(m\pi z / H) ,$$
$$\hat{\theta} = \sum_{m=1}^{\infty} \Theta_{lm} e^{\beta_{lm} x} \sin(m\pi z / H) . \tag{12}$$

Here m is a mode index, and the characteristic height scales are $\mathrm{m^{-1}}$. Put Eq.(12) into Eq.(8), we then obtain the secular equation

---

①The Fourier series does not converge to the right values at $z = 0$ and $z = H$. All the series below should be understood to be evaluated for $0 < z < H$ only, and the limits $z \to 0$ or $z \to H$ are taken afterwards if necessary.

②The boundary conditions on ψ demand that it is expanded in a sine series. Eq.(8) then specifies how each function is expanded.

$$\begin{bmatrix} \chi_l & f(m\pi/H) & 0 \\ f(m\pi/H) & \chi_l[\beta_{lm}^2-(m\pi/H)^2] & \beta_{lm} \\ 0 & -\beta_{lm}N^2 & i\omega \end{bmatrix} \begin{bmatrix} V_{lm} \\ \Psi_{lm} \\ \Theta_{lm} \end{bmatrix} = 0 \tag{13}$$

for each m, where $\chi_l = i\omega + k_1$. A nontrivial solution is

$$\beta_{lm}^2 = \left(\frac{m\pi}{H}\right)^2 \left\{\frac{(1-k_1\eta_l)(1+\hat{f}^2\eta_l^2)}{1-k_1\eta_l+N^2\eta_l^2}\right\}, \tag{14}$$

where $\eta_l = \chi_l^{-1} = (i\omega + k_1)^{-1}$. The factor in the large brackets in (14) is independent of m, so the lateral extent of each mode scales is $\beta_{lm}^{-1} \propto m^{-1}$, in other words, in the same manner as the vertical scale, which is reasonable. Of the two solutions for β_{lm}, we only take the one with $Re\beta_{lm} \geqslant 0$, in order to ensure that the solution remains bounded as $x \to -\infty$. $Re\beta_{lm}$ controls the decay of the perturbation with distance from the coastline, while Im β_{lm} controls the oscillation with x.

After getting β_{lm}, the coefficients in the expansion of $\hat{v}$, $\hat{\psi}$, $\hat{\theta}$ can all be expressed in terms of say Θ_{lm}.

$$\begin{aligned} U_{lm} &= \frac{i\omega}{\beta_{lm}N^2}\left(\frac{m\pi}{H}\right)\Theta_{lm}, \\ V_{lm} &= -\frac{i\omega}{\beta_{lm}N^2} f\eta_l \left(\frac{m\pi}{H}\right)\Theta_{lm}, \\ \psi_{lm} &= \frac{i\omega}{\beta_{lm}N^2}\Theta_{lm}. \end{aligned} \tag{15}$$

A similar expansion is adopted for the sea ($x > 0$) but with frictional parameter k_s and heating rate $Q_s e^{-\delta z}$, and the modes are labelled as m, where again $m = 1, 2, \cdots$. Also, to ensure that the solution remains bounded as $x \to \infty$, we need to take β_{sm} to be the root with a negative real part. The coefficient η_s is introduced in a similar manner. We note that $\beta_{lm} \neq \beta_{sm}$, indicating an asymmetry in the penetration of the effect landwards and seawards. This will be discussed in greater detail in the next section.

2.3 *Matching across the coastline*

Now we match the two solutions across the coastline $x = 0$. Obviously, ψ has to be continuous, so

$$\frac{\Theta_{lm}}{\beta_{lm}} = \frac{\Theta_{sm}}{\beta_{sm}}. \tag{16}$$

Also the continuity of θ across $x = 0$①gives

$$\left[\sum_m \Theta_{lm} e^{\beta_{lm}x} \sin\left(\frac{m\pi}{H}z\right) - \frac{iQ_1}{\omega}e^{-\delta z}\right]_{x=0} = \left[\sum_m \Theta_{sm} e^{\beta_{sm}x} \sin\left(\frac{m\pi}{H}z\right) - \frac{iQ_s}{\omega}e^{-\delta z}\right]_{x=0}, \tag{17}$$

①More precisely, we retain ξ in Eq.(3); this guarantees that θ is continuous across $x = 0$. The expression for θ is matched, and then $\xi \to 0$ is taken. This then results in Eq.(17). Thus Eq.(17) is valid when ξ is sufficiently small.

leading to

$$\sum_m \Delta_m \sin\left(\frac{m\pi}{H} z\right) = \frac{i\Delta Q}{\omega} e^{-\delta z} , \tag{18}$$

where $\Delta_m = \Theta_{lm} - \Theta_{sm}$, $\Delta Q = Q_l - Q_s$.

Projecting the right hand side of Eq.(18), we find the coefficients for the potential temperature difference are

$$\Delta_m = \frac{i\Delta Q}{\omega} \alpha_m , \tag{19}$$

where α_m is a purely geometrical factor

$$\alpha_m = \frac{2}{H} \left\{ \frac{m\pi / H}{(m\pi / H)^2 + \delta^2} [1 - (-1)^m e^{-\delta H}] \right\} , \tag{20}$$

which is asymptotically $\propto m^{-1}$. From Eq.(16) and Eq.(19), Θ_{lm} and Θ_{sm} can be found.

$$\Theta_{lm} = \frac{i\Delta Q}{\omega} \alpha_m \left(\frac{\beta_{lm}}{\beta_{lm} + \beta_{sm}} \right)$$

$$\Theta_{sm} = \frac{i\Delta Q}{\omega} \alpha_m \left(\frac{\beta_{sm}}{\beta_{lm} + \beta_{sm}} \right) \tag{21}$$

When this result is substituted into the series solution, the entire flow field is determined.

3. Structure of sea–land breeze

In this section, we discuss the general properties of the solution found for the sea–land breeze circulation, using the "standard" parameters in Table 1. We note, first of all, that although the potential temperature θ peaks at 1800 LST in the particular solution (2.9), it peaks near noon in the full solution, which is reasonable.

Driving force

From Eq.(21), Θ_{lm}, Θ_{sm} and all the other variables describing the circulation are directly proportional to the difference in the heating rates ΔQ. In other words, there is no sea–land breeze if the land and the sea are subjected to the same diurnal heating. This is the most important feature of the model.

Vertical distribution

The vertical structure is expressed as a sum of harmonics, or waves, with wavelengths $\lambda_m = 2H / m$. The $m = 1$ term has no node in the model domain $(0, H)$, and is a barotropic mode. The $m \geqslant 2$ modes are baroclinic.

Horizontal distribution

The horizontal distribution in each mode is determined by β_{lm} and β_{sm}, and may be characterized by horizontal scales

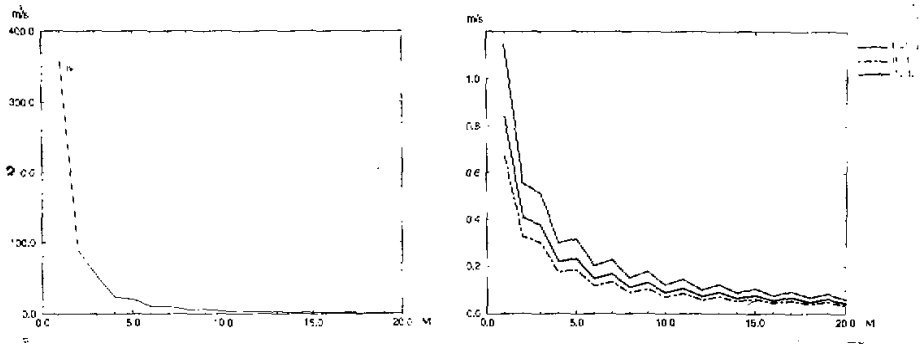

Fig. 2. The amplitude of various quantities versus the mode number m. (a) The amplitude of stream function $|\Psi_m|$. (b) The amplitude of the horizontal velocity perpendicular to the coast $|U_{lm}|$; the amplitude of the horizontal velocity along the coast over land $|V_{lm}|$; the amplitude of horizontal velocity along the coast over sea $|V_{sm}|$.

$$D_{lm} = \frac{1}{Re\beta_{lm}} \quad ,$$

$$D_{sm} = \frac{1}{Re\beta_{sm}} \quad , \tag{22}$$

which define the distances (respectively landwards and seawards of the coastline) where each mode decays by a factor of e. The fundamental mode has a horizontal extent

$$L_1 = D_{l1} + D_{s1} \approx 80 \text{ km} + 200 \text{ km} = 280 \text{ km} \quad . \tag{23}$$

When all modes are summed, the overall wind field has a shorter horizontal length scale of about 50 to 100 km, which is broadly consistent with observations (Atkinson, 1984).

Figs. 2a and 2b give the amplitudes of ψ, u, v_l and v_s at $x = 0$ versus the mode number m. The amplitudes decrease rapidly with m, and in practice, all numerical results reported are calculated by truncating the sum at $m = 20$.

Wind direction

For each mode, the ratio of the wind speeds along and normal to the coastline is given by

$$\frac{|V_{lm}|}{|U_{lm}|} = f|\eta_l| = \frac{f}{\sqrt{\omega^2 + k_l^2}} \quad . \tag{24}$$

The ratio is larger (i.e., the wind has a larger component along the coastline) at higher latitudes; the ratio also decreases as the frictional force increases. If friction could be neglected, then

$$\frac{|V_{lm}|}{|U_{lm}|} = 2\sin\varphi \leqslant 2 \quad , \tag{25}$$

where φ is the latitude. We note from Eq.(24) that the ratio is independent of m, and in fact the phase of the ratio is also independent of m. So the overall wind components u and v (the sum over all modes) are given by the same ratio as Eq.(24). However, because of the phase difference, the actual wind speeds v and u at any time are *not* given by this ratio.

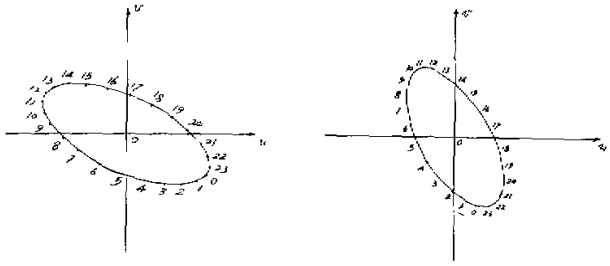

Fig. 3. The diuranal variation of the wind speed 1 km inland, at various times labelled by hours LST. The normalization is arbitrary, since all winds are proportional to the amplitude of ΔQ. (a) At 22°N. (b) At 60°N.

Diurnal variation

Figs. 3a and 3b give the diurnal variation of wind speed 1 km inland, at latitudes 22°N and 60°N respectively, labelled by hours according to the local sun time (LST). It is assumed that the heating rate is maximum at 1200 LST.

These figures show that the wind speed is minimum at about 0500 and 1700 LST (near sunrise and sunset), and maximum at about 1100 and 2300 LST (near noon and midnight), with some small variations with latitude. The wind component v is larger at higher latitudes, which is also evident from the dependence on f in Eq.(24).

Fig. 4a gives the diurnal variation of wind field at latitude 22°N, using parameters as in Table 1. The horizontal axis x is the distance from the coastline, and the vertical axis is time in hours LST. The wind direction is seen to change after sunrise, from a land breeze to a sea breeze. At 0900 LST, the wind speed increases substantially. The sea breeze reaches its maximum speed (of about 5 m s^{-1}) at about 1200 LST. After 1500 LST the wind speed decreases. The wind changes back to a land breeze at 1800 LST. At about 2100 LST, the land breeze intensifies and reaches its maximum speed (of about 5 m s^{-1}) at about 2400 LST. The land breeze then decreases until sunrise.

Spatial profile

From Fig. 4a, the sea–land breeze extends further out to the sea than into the land, essentially because different values of the frictional parameter have been used. The convergence zone occurs over land while the divergence zone occurs over sea during the sea breeze phase. This situation is reversed for the land breeze phase.

Figs. 4b and 4c show the $x - z$ profile of the stream function at 1200 LST (sea breeze maximum) and 1800 LST (transition between sea breeze and land breeze), respectively, using the same parameters as in Fig. 3a. From Fig. 4b, the wind speed decreases vertically and the vertical extent is about 300 m. The direction of flow is reversed above that height. The stream function is qualitatively the same as shown in Fig. 58 of Atkinson (1984).

At 1800 LST (Fig. 4c), the pattern of the circulation is quite different. A weak circulation from sea to land is developed ($u > 0$) at the coast. However, away from the coast, $u < 0$, it is still in the original sea breeze phase. Thus, the sea–land breeze develops and changes direction starting from the coast.

Figs. 5a and 5b give the wind components u and v respectively, 1 km inland at various heights. The horizontal axis is time in hours. The vertical axis is height. These two figures

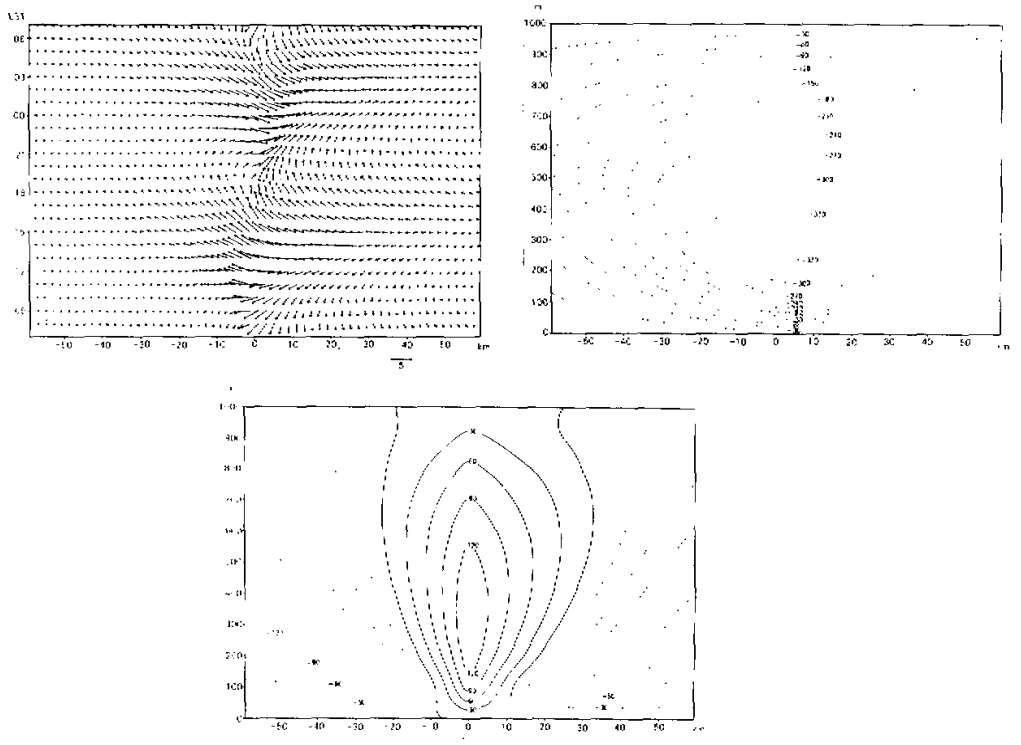

Fig. 4. Wind distribution at 22°N. (a) Wind vectors shown vs distance from the coast (horizontal axis) and time in hours LST (vertical axis). The arrow below the figure corresponds to 5 m s^{-1}. (b) The stream function ψ at 1200 LST (sea breeze maximum) as a function of the distance x from the coast (horizontal scale) and height z (vertical scale). (c) The stream function ψ at 1800 LST (transition from sea breeze to land breeze) as a function of the distance x from the coasr (horizontal scale) and height z (vertical scale).

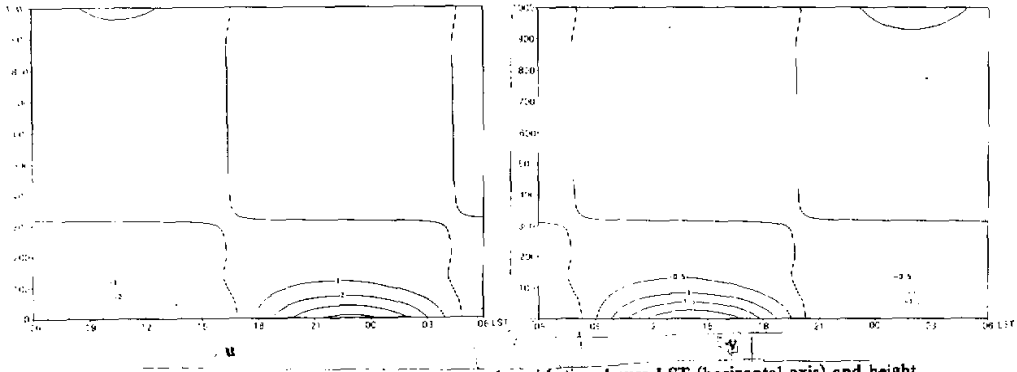

Fig. 5. The variation of the wind components u and v with time hours LST (horizontal axis) and height z (vertical axis), at a position 1 km inland. (a) The wind component u along the coast. (b) The wind component v alomg the coast.

show that the sea breeze occurs in the lower parts of the atmosphere, decreasing in amplitude vertically. At a height of 300 m, the direction of the circulation is reversed.

The height at which the circulation reverses depends physically on the height of the inversion layer (represented by H) and the vertical heating profile (represented by δ^{-1}), and can range from a hundred metres (the present model) to over 1 km (see Fig. 1).

The two components u and v have a phase difference, and v reaches maximum later than u. Assuming the coast runs along the east–west direction with the sea to the south, the strongest sea breeze is from the SW and strongest land breeze from the NE. The result agrees with the observed data as shown in Fig. 1. From the above results, the output of this analytic model agrees with data and can represent the structure and the evolution of sea–land breeze very well.

4. Dependence on the parameters

4.1 *Heating rate*

Fig. 6 shows the wind components u and v 1 km inland, and illustrates how they vary with ΔQ. The parameters are shown in Table 1. As both the sea and the land begin to heat up after sunrise, the sea breeze is developed and the wind speed increases as the heating increases. At 1200 LST, the sea–land heating difference is maximum and so is the wind speed, with a value of about 4.6 m s^{-1}. The difference of heating rates then decreases, and the sea breeze also decreases. The difference of heating rates changes sign after sunset, so the land breeze develops and intensifies. The heating rates have a maximum difference at midnight and the land breeze also reaches its maximum. After that the land breeze weakens until sunrise.

The heating rate was assumed to be a sinusoidal function, which agrees reasonably with observation in the daytime, but is not realistic at night. To have a better representation of the heating rate, different harmonics $e^{in\omega t}$ have to be considered, with both the fundamental mode ($n = 1$, period of one day) and other modes ($n > 1$, period shorter than one day). However, the fundamental mode accounts for the main contribution and produces the main features of the sea–breeze variation in time.

The influence of the vertical distribution of Q on the sea–land breeze is interesting. As an example, we use parameters in Table 1, but with δ changed from 2×10^{-3} m^{-1} to 4×10^{-3} m^{-1}. The surface wind field (Fig. 7a) is more or less the same as shown in Fig. 3. The wind speed is smaller. The stream function diagram at 1200 LST (Fig. 7b) shows a lower

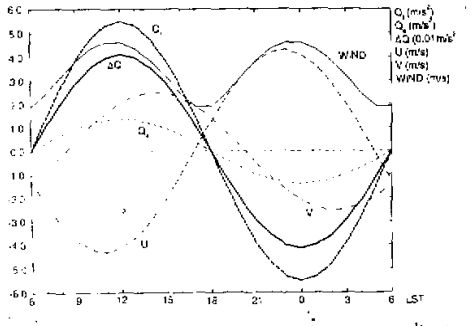

Fig. 6. The variation of the differential heating rate ΔQ (unit of m s^{-1}), the wind components u and v (unit of m s^{-1}) vs time in hours LST (horizontal axis). the winds refer to a postion 1 km inland.

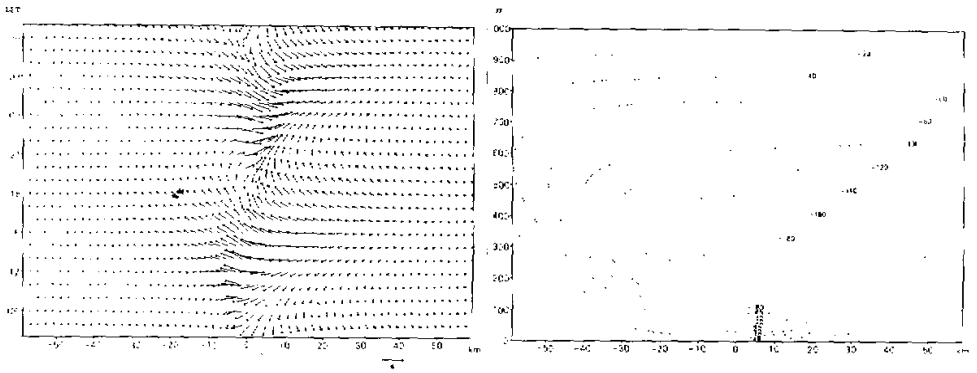

Fig. 7. The diurnal variation of the wind field at 22°N. (a) The wind vector as a function of the distance from the coastline (horizontal axis) and time in hours LST (vertical axis). The arrow below the figure corresponds to 4 m s^{-1}. (b) The stream function ψ at 1200 LST (sea breeze maximum) as a function of the distance x from the coast (horizontal axis) and height z (vertical axis).

vertical extent of the sea–land breeze circulation. When δ is increased to $10^{-2}m^{-1}$, the speed of the sea–land breeze not only decreases but its vertical extent also decreases, to about 100 m (diagrams not shown). From the above results, we see that the vertical extent of sea–land breezes varies with δ^{-1}.

4.2 *Latitude*

Table 2 gives the values of D_{fl} and D_{sl} at different latitudes, using parameters as in Table 1. It also gives the amplitude of the stream function Ψ of the barotropic mode ($m = 1$). From the table, as the latitude increases, D_{fl} and D_{sl} decrease, more rapidly at lower latitudes. The amplitude of the stream function Ψ has a maximum value at about 30° latitude. Since the amplitude of u is directly proportional to Ψ, as a result of the two reasons cited above, sea–land breezes are found more frequently at mid–latitudes. The wind speed and horizontal extent are also larger. This result agrees with observation.

Table 2. The dependence on latitude

Latitude	0°	15°	22°	30°	45°	60°	75°	90°	
D_{fl}	117	96	80	63	44	34	30	29	km
D_{sl}	442	305	203	104	44	31	27	26	km
$\lvert\Psi\rvert$	318	340	364	379	291	232	205	197	$m^2\ s^{-1}$

Fig. 8a gives the diurnal variation of the surface wind at 60°N latitude, using the parameters in Table 1 (except for the Coriolis parameter f). Comparing Fig. 3a with Fig. 8a, the flow field is not the same. The horizontal extent is smaller and the wind component v is larger in Fig. 8a than that in Fig. 3a. Fig. 8b gives the stream function diagram at 1200 LST. Compared with Fig. 4b, the stream function is weaker and the centre of the circulation has shifted landwards.

With the same heating rate, a weaker and shallower sea–land breeze is developed at higher latitudes because the Coriolis force is larger. The force changes the wind direction

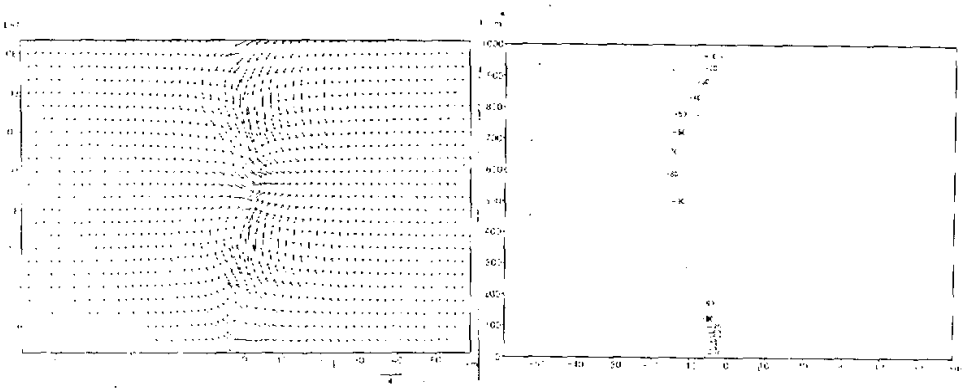

Fig. 8. The diurnal variation of the wind field at 60°N. (a) The wind vector as a function of the distance from the coastline (horizontal axis) and time in hours LST (vertical axis). The arrow below the figure corresponds to 4 m s^{-1}. (b) The stream function ψ at 1200 LST (sea breeze maximum) as a function of the distance x from the coast (horizontal axis) and height z (vertical axis).

much more and the breeze cannot penetrate as much inland. The same reasoning applies to the land breeze. Actually, there are fewer sea–land breezes at higher latitudes, not only because of the above reason, but also because the heating rate is weaker.

4.3 *Stratification*

Table 3 gives the values of $|\Psi|$, D_{l1} and D_{s1} at 22°N and 60°N but with various values of stratification N^2, with other parameters as in Table 1. As the stability of stratification increases, D_{l1} and D_{s1} also increase. The horizontal extent also increases, but $|\Psi|$ decreases.

Table 3. The dependence on the stability of stratification at 22°N and 60°N

Latitude	22°N										
N^2	0.01	0.03	0.05	0.07	0.1	0.30	0.50	0.70	1.00	2.00	10^{-4} s^{-1}
D_{l1}	7.95	13.83	17.87	21.15	25.29	43.82	56.58	66.95	80.02	113.1	km
D_{s1}	20.24	35.16	45.42	53.76	64.27	111.36	143.77	170.11	203.33	287.5	km
$\|\Psi\|$	3635	2102	1629	1377	1152	665	515	436	364	258	m^2 s^{-1}
Latitude	66°N										
N^2	0.01	0.03	0.05	0.07	0.1	0.30	0.50	0.70	1.00	2.00	10^{-4} s^{-1}
D_{l1}	3.42	5.94	7.67	9.09	10.86	18.82	24.30	28.75	34.36	48.6	km
D_{s1}	3.12	5.41	6.98	8.26	9.87	17.11	22.10	26.14	31.25	44.1	km
$\|\Psi\|$	2370	1336	1035	875	732	423	238	277	232	164	m^2 s^{-1}

Fig. 9a gives the diurnal variation of the surface wind at 22°N, using parameters as in Table 3 and $N^2 = 10^{-5}$ s^{-2} instead of 10^{-4} s^{-2}. Comparing Fig. 3a with Fig. 9a, the wind speed is doubled: the former is about 5 m s^{-1}, while the latter is about 10 m s^{-1}.

Fig. 9b gives the stream function diagram at 1200 LST, using the results of Fig. 9a. Comparing Fig. 4b with Fig. 9b, the centre of the stream function increases to 3 times the original value when the stability of stratification is weaker. The speed of the sea breeze increases, but the horizontal extent decreases. Comparing the stream function diagrams at 1800 LST, the result is about the same. This comparison indicates that with weaker stratification

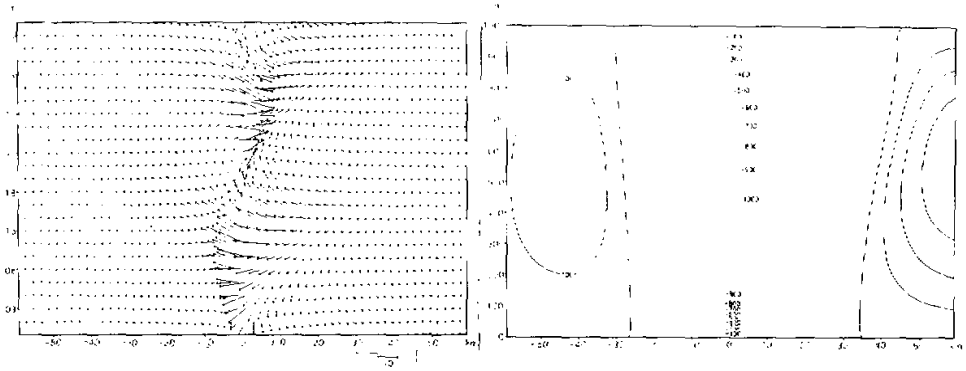

Fig. 9. Same as Fig. 7, but N^2 changed from 10^{-4} s^{-2} to 10^{-5} s^{-2}.

stability, the speed of sea–land breezes is stronger but it decays more rapidly with the distance from the coast. The wind speed is higher along the coastline and by continuity, so is the vertical wind speed. Thus rainfall or thunderstorm tends to occur when the stratification stability is weaker. This result should be of interest in weather forecasting.

4.4 *Frictional parameter*

Many studies of the sea–land breeze circulation use the same frictional parameter for the sea and the land; however, the roughness is not the same in the two cases. Since the vertical extent of the sea–land breeze circulation is not too high, the frictional parameter of the land and the sea can be assumed to be constants in each domain. In the following discussion, we keep $k_s = 0.25k_1$, and vary the two together.

Table 4 gives the values of D_{l1}, D_{s1} and Ψ at latitudes 22°N and 60°N with different values of the frictional parameters in unit of day^{-1}, using other parameters as in Table 1. From Table 4, the frictional parameters have a larger effect on the sea–land breeze at lower latitudes. The larger the friction, the smaller the horizontal extent of the sea–land breeze. At higher latitudes, the frictional parameter does not affect the sea–land breeze as much. It can be said that the horizontal extent at lower latitudes is more sensitive than that at higher latitudes to changes of the frictional parameter. The frictional force decreases the stream function and also reduces the wind speed.

Table 4. The dependence on the frictional parameter at 22°N and 60°N. ($k_s = 0.25k_1$)

Latitude	22°N							
k_1	*1*	*2*	*5*	*7*	*10*	*15*	*20*	day^{-1}
D_{l1}	247.25	139.74	80.02	67.84	56.83	45.77	38.94	km
D_{s1}	937.08	474.09	203.33	154.54	119.45	93.17	80.02	km
$\lvert\Psi\rvert$	489.9	451.9	364.4	329.5	293.2	253.4	226.8	$m^2\ s^{-1}$
Latitude	60°N							
k_1	*1*	*2*	*5*	*7*	*10*	*15*	*20*	day^{-1}
D_{l1}	31.14	31.69	34.36	35.94	37.02	36.05	33.69	km
D_{s1}	30.96	31.00	31.25	31.52	32.06	33.18	34.36	km
$\lvert\Psi\rvert$	238.4	237.4	231.6	226.5	217.8	203.3	190.4	$m^2\ s^{-1}$

From the above reason, it can be seen that if we use different frictional parameters over

the land and the sea, the horizontal extent will be different in the two cases: larger over the sea but smaller over the land. The sea–land breeze circulation is not symmetrical. From the previous figures, this situation can be clearly observed.

5. Conclusions

This study assumes that the land and the sea are subjected to different heating rates and have different frictional parameters. The heating rate is described as a single sinusoidal function with a period of one day. Using the Boussinesq approximation, an analytic solution of a linearized two-dimensional baroclinic model is studied. The conclusions are as follows.

(1) The speed of the sea–land breeze is directly proportional to the difference in the heating rates. When the sea and the land are heated, a sea breeze occurs, peaking at noon. As the sea and the land cool off at night, a land breeze occurs, peaking at midnight. These results agree qualitatively with observation.

(2) The vertical extent of the sea–land breeze varies with both H and δ^{-1}.

(3) The sea–land breeze depends sensitively on the latitude. With the same heating, the horizontal extent is much larger at lower latitudes than at higher latitudes, and the speed is also higher.

(4) When the stratification of stability is weak, the wind speed is higher for the sea–land breeze. The horizontal extent is smaller.

(5) The frictional force reduces the wind speed. At lower latitudes, the greater the frictional force, the smaller the horizontal scale of the sea–land breeze. However, the horizontal scale is not sensitive to the frictional force at higher latitudes. With different frictional parameters over sea and land, the horizontal extent becomes asymmetric.

In this study, the heating rate is a sinusoidal function with a period of one day. This has the effect that the two halves of the day are mirror images, so that the land breeze and the sea breeze have equal strengths and opposite directions. This feature is not realistic, and should be improved by taking a more realistic heating function and keeping more temporal harmonics ($n > 1$).

Assuming constant values of the frictional force over land and sea and a straight coastline are also not entirely realistic. Also, the effect of prevailing background wind in the sea–land breeze is not included. These should be improved in further studies. Finally, with strong sea–land breezes, gravity currents occur (Sha et al. 1991), which require the non-linear governing equations, for which one may need to resort to numerical simulations.

We thank Mr C. Y. Lam and Mr H. T. Poon of Hong Kong Observatory for discussions, especially about the sea–land breeze circulation observed around Hong Kong and the Zhujiang estuary. We have benefited from insight gained from a numerical model for the Hong Kong region developed by Prof. Zhang Lifeng, and also a simplified numerical model for the Zhujiang River estuary developed by Mr Lam Wang Yuen. Mr Ngan Shiu Fai gave valuable help in the preparation of the manuscript. This work is supported in part by the Croucher Foundation of Hong Kong.

REFERENCES

Atkinson, B. W. 1984: *Meso-scale Atmospheric Circulations*. Academic Press, London.

Dalu, G. A., and R. A. Pielke. 1989: An analytical study of the sea breeze. *J. Atmos. Sci.*, **46**, 1815–1825.

Defant, F. 1951: Local winds. *Compendium of Meteorology*, American Meteorology Society, 655–672.

Flohn, H. 1969: Local wind systems. *Climatology*, Vol. 2. Ed. H. Flohn, Elsevier, Amsterdam, 139–171.

Halley, E. 1886: An historical account of the trade-winds and monsoons observable in the seas between and near the

tropics with an attempt to assign the physical cause of said winds. *Phil. Trans. R. Soc. London*, **26**, 153–168.

Haurwitz, B. 1947: Comments on the sea-breeze circulation. *J. Meteor.*, **4**, 1–8.

Lu, R., and R. P. Turco, 1994: Air pollutant transport in a coastal environment. Part I: Two-dimensional simulations of sea-breeze and mountain effects. *J. Atmos. Sci.*, **51**, 2285–2308.

Niino, H. 1987: The linear theory of land and sea circulation. *J. Meteor. Soc. Japan*, **65**, 901–920.

Rotunno, R. 1983: On the linear theory of land and sea breeze. *J. Atmos. Sci.*, **40**, 1999–2009.

Sha, W., T. Kawamura, and H. Ueda, 1991: A numerical study on sea/land breezes as a gravity current: Kelvin-Helmholtz billows and inland penetration of the sea-breeze front. *J. Atmos. Sci.*, **48**, 1649–1665.

Simpson, J. E. 1994: *Sea Breeze and Local Winds*. 1st edition, Cambridge University Press, New York

Smith, R. K., N. Crook, and G. Roff, 1982: The morning glory: an extraordinary atmospheric undular bore. *Q. J. R. Meteor. Soc.*, **108**, 937–956.

Sun, W. Y., and I. Orlanski, 1981: Large mesoscale convection and sea breeze circulation. Part II: Nonlinear Numerical Model. *J. Atmos. Sci.*, **38**, 1694–1706.

Walsh, J. E. 1974: Sea breeze theory and applications. *J. Atmos. Sci.*, **31**, 2012–2026.

Yan, H., and R. A. Anthes, 1987: The effect of latitude on the sea breeze. *Mon. Weather Rev.*, **115**, 939–956.